PERGAMON

Chemical Engineering Science 58 (2003) 4605–4617

Chemical Engineering Science

www.elsevier.com/locate/ces

Monte-Carlo simulations of surface and gas phase diffusion in complex porous structures

Jeffrey M. Zalc[a], Sebastián C. Reyes[b], Enrique Iglesia[a,*]

[a] *Department of Chemical Engineering, University of California at Berkeley, Berkeley, CA 94720, USA*
[b] *ExxonMobil Research and Engineering Co., Route 22 East, Annandale, NJ 08801, USA*

Received 24 April 2003; received in revised form 29 July 2003; accepted 30 July 2003

Abstract

A new procedure for estimating surface diffusivities and tortuosities within realistic models of complex porous structures is reported. Our approach uses Monte-Carlo tracer methods to monitor mean-square displacements for molecules restricted to wander on pore walls within model random mesoporous solids typical of those used as adsorbents, heterogeneous catalysts, and porous membranes. We consider model porous solids formed from initial packings of spheres with unimodal, Gaussian, or bimodal distributions of size; changes in pellet porosity are achieved by increasing microsphere radii and by randomly removing spheres from highly densified packings in order to simulate densification and coarsening, respectively. Geometric tortuosities for the surface phase reached large values at void fractions near 0.04 and 0.42 for densified solids; the surface tortuosity gave a minimum value of 1.9 at a void fraction of ~0.26. These high tortuosities correspond to percolation thresholds for the void and solid phases, which in turn reflect packing densities at which each phase becomes discontinuous. Surface tortuosities for coarsened solids at low void fractions were similar to those in densified solids; however, at void fractions above ~0.3, surface tortuosities of coarsened solids increased only gradually with void fraction, because coarsening retains significant overlap among spheres at void fractions above those giving disconnected solids in densified structures. Simulations of bulk diffusion within voids were used to compare the transport properties and connectivity of the void space with those of surfaces that define this void space. Surface and void tortuosities were similar, except for void fractions near the solid percolation threshold, because unconnected solid particles interrupt surface connectivity but not gas phase diffusion paths. Surface and void tortuosities were also similar for channels within linear chains of overlapping hollow spheres as both tortuosities increased with decreasing extent of sphere overlap. These simulations provide a basis for estimates of surface and void tortuosities, which are essential in the interpretation and extrapolation of diffusion rates in complex porous media. Surface and void diffusivity estimates differed significantly from those obtained from lattice and capillary models of complex porous structures.

Keywords: Simulation; Transport processes; Porous media; Diffusion; Surface tortuosity; Monte-Carlo

1. Introduction

The transport properties of porous materials are critical for their function in heterogeneous catalysis (Satterfield, 1970; Wakao & Smith, 1962; Weisz & Hicks, 1962), non-catalytic gas–solid reactions (Dogu, 1981; Wen, 1968), membrane transport (Baker, 2002; Kong, Kim, Lee, Shul, & Lee, 2002), and adsorption processes (Ruthven, 1984). The large surface areas required for high densities of adsorption or catalytic sites can impair efficient access to such sites by reactants and the required removal of reaction products, because of complex interconnections among the small voids responsible for these high surface areas. Intrapellet transport restrictions limit the rates and selectivities for many chemical reactions catalyzed by solids (Aris, 1975; Froment & Bischoff, 1990) and may lead to undesired localized phenomena, such as exotherms, which can lead to catalyst deactivation by sintering or to carbon formation (Bartholomew, 2001). Rigorous guidance for the design of porous catalysts, membranes, and adsorbents requires detailed knowledge about the dynamics of all transport processes involved in the exchange of molecules between the external fluid phase and the intraparticle void and surface structures.

* Corresponding author. Tel.: +1-510-642-9673; fax: +1-510-642-4778.
E-mail address: iglesia@cchem.berkeley.edu (E. Iglesia).

0009-2509/$ - see front matter © 2003 Elsevier Ltd. All rights reserved.
doi:10.1016/j.ces.2003.07.008

In heterogeneous reactors, transport of chemical species occurs over a wide range of length and time scales (Lee, 1985; Raimondeau & Vlachos, 2002), as illustrated in Fig. 1. At the largest scales, hydrodynamic effects (Figs. 1a and b) influence flow patterns and mass transfer between the bulk fluid and the porous solids. Transport within intrapellet voids occurs via bulk (Fig. 1c) or Knudsen diffusion (Fig. 1d), depending on the relative magnitude of the mean free path of molecules, λ, and the mean pore size, $\bar{r}_p$. When molecules adsorb and move along pore walls, surface diffusion contributes an additional transport path (Fig. 1e). Surface diffusion involves motion of adsorbed species under the influence of a potential energy field imposed by the surface; for chemisorbed species, such migration processes can involve the sequential formation and cleavage of bonds with surfaces (Somorjai, 1972; Tsong, 2001). The relative contributions of gas phase and surface diffusion processes depend on the dimensions, availability, and connectivity of the void space, on the mobility and mean free paths on the surface and in the void space, and on the connectivity and roughness of the surfaces that define the intraparticle voids.

Experimental studies have shown that surface diffusion contributes significantly to the total diffusive flux in both mesoporous and microporous systems (Carman & Malherbe, 1950; Eberly Jr., & Vohsberg, 1965; Prasetyo, Do, & Do, 2002; Richard, Favre, Tondeur, & Nijmeijer, 2001; Tuchlenski, Uchytil, & Seidel-Morgenstern, 1998). The contribution of surface diffusion increases as surface concentrations of adsorbed species increase from sub-monolayer to multi-layer coverages (Choi, Do, & Do, 2001; Gilliland, Baddour, Perkinson, & Sladek, 1974; Jaguste & Bhatia, 1995). Even well below a monolayer, surface diffusion contributes to overall transport rates in porous carbon (Ash, Barrer, & Pope, 1963), silica (Schneider & Smith, 1968), and MoS_2 (Reed Jr., & Butt, 1971). Experimental surface diffusivities are estimated from differences in transport rates for molecules and conditions that lead to significant or negligible surface transport (Barrer & Grove, 1951a, b). This indirect approach and our limited knowledge about molecule-surface interactions has prevented the separation of intrinsic surface mobilities from morphological effects of surface connectivity within complex porous structures.

When surface and gas phase diffusion occur concurrently, the steady-state diffusion flux, N, depends on the relevant driving forces in the surface and gas phases:

$$N = N_g + N_s = -\left[D_{e,g}\frac{C_g}{f_g}\frac{\mathrm{d}f_g}{\mathrm{d}x} + a_v D_{e,s}\frac{\mathrm{d}(\ln f_s)}{\mathrm{d}(\ln C_s)}\frac{\mathrm{d}C_s}{\mathrm{d}x}\right], \quad (1)$$

where N_g is the gas phase diffusive flux, N_s is the surface diffusive flux, $D_{e,g}$ is the effective gas phase diffusivity, $D_{e,s}$ is the effective surface diffusivity (both with (length)^2/time units), C_g is the gas phase concentration (moles per unit void volume), C_s is the surface concentration (moles per unit surface area), a_v is the surface-to-volume ratio, x is the direction of net motion, and f_s and f_g are the fugacities of the diffusing species in the thermodynamically non-ideal surface and gas phases, respectively (Reyes, Sinfelt, & DeMartin, 2000). The assumptions of an ideal gas phase ($f_g = C_g/RT$) and adsorption–desorption equilibrium ($f_s = f_g$) lead to

$$N = N_g + N_s = -\underbrace{\left[D_{e,g} + a_v D_{e,s}\frac{C_s}{C_g}\right]}_{D_e}\frac{\mathrm{d}C_g}{\mathrm{d}x}, \quad (2)$$

where D_e is the overall effective diffusivity. We note that C_s is related to C_g through an adsorption isotherm that may or may not reflect a thermodynamically ideal adsorbed phase and that the ratio C_s/C_g becomes the Henry's law constant for conditions leading to a linear relation between gas and surface concentrations.

Transport properties of porous solids have been treated using interconnected bundles of tortuous capillaries and regular lattices as convenient models of the void structure. For combined gas phase and surface diffusion, an effective diffusivity can be described in terms of the diffusivities associated with an equivalent capillary and of tortuosity factors for the void and surface phases:

$$D_e = \frac{D_g\phi}{\tau_g} + \frac{D_s}{\tau_s}a_v\frac{C_s}{C_g}. \quad (3)$$

D_g and D_s are gas phase and surface diffusivities, respectively, in equivalent capillaries; they depend on properties of molecules, such as their velocity in the fluid phase and their binding energy and mobility as diffusing species on surfaces. The terms τ_g and τ_s denote the gas (void) and surface tortuosities, defined as the length of the equivalent capillary required in order to describe effective diffusivities in the void and surface phases, respectively. As Eq. (3) clearly shows, the net contribution of the surface to overall transport also depends on the surface-to-volume ratio and on the adsorption isotherm (Reyes et al., 2000).

Computational studies of gas diffusion within porous solids have often used random aggregates of spheres (Akanni, Evans, & Abramson, 1987) or cylinders (Burganos & Sotirchos, 1989; Tomadakis & Sotirchos, 1993) to describe the details of the porous medium. Specifically, partially overlapped random-loose packings of spheres can be used to simulate the structure and void phase transport properties of coarsened and densified porous solids (Reyes & Iglesia, 1991a, 1993). The impact of pore space structure on surface diffusion in porous solids has received less attention (Bhatia, 1988; Ho & Strieder, 1981). The few available treatments address lattice diffusion near obstacles on flat surfaces (Pekalski & Ausloos, 1995) or random walk simulations on unobstructed curved surfaces (Holyst, Plewczynski, Aksimentiev, & Burdzy, 1999), which do not provide realistic descriptions of surface transport within complex structures.

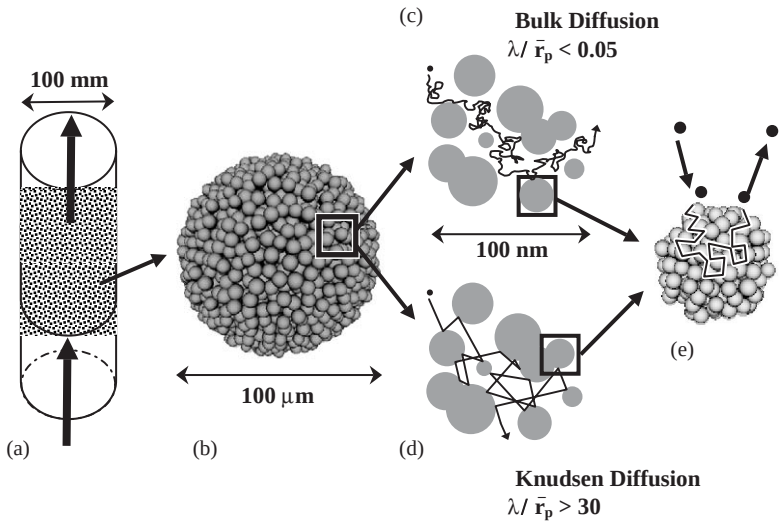

Fig. 1. Schematic diagram of the range of length and time scales over which mass transport occurs in complex porous structures held within contacting flow devices. Hydrodynamic flow driven by local pressure gradients at device length scales (a), intraparticle mass transport (b) involving bulk (c) or Knudsen (d) gas phase diffusion and driven by local concentration gradients. Surface diffusion (e) occurring over atomic length scales as adsorbed molecules move between atomic positions of surfaces.

Here, we describe an algorithm for monitoring random walks on exposed surfaces of randomly packed and overlapped spheres, which provide realistic representations of complex solids. Effective surface diffusivities are estimated using tracer methods that probe the geometric connectivity and tortuosity of the surface phase. These estimates are compared with those from tracer simulations within the void space to provide a complete description of combined void and surface transport properties for these porous structures.

2. Algorithms for porous structure assembly and for simulating effective diffusivities for surfaces and voids

Simulations of transport within porous solids require: (i) appropriate methods to represent realistic porous structures and (ii) efficient algorithms to monitor tracer motion within the voids and on the surfaces that constrain these voids. Our previous studies have focused on the synthesis and characterization of such porous structures and on simulations of the transport properties of their void space (see Reyes & Iglesia, 1991a, b and references therein); therefore, we describe these procedures only briefly here. The current study extends this previous work to diffusion on surfaces, while concurrently providing a rigorous comparison of the transport properties of the void and surface phases.

2.1. Structural models of porous solids

Scanning electron micrographs of SiO_2 and TiO_2 porous solids are shown in Fig. 2. These structures are typical of solids formed by sol-gel, precipitation, and combustion methods. The internal structure of pellets or agglomerates formed by these methods consists of microspheres overlapped to various extents. When these microspheres are non-porous, their interparticle space provides the only available diffusion path; for porous microspheres, intraparticle voids also contribute to this diffusion path. The computational assembly of these representative structures involves packing of spheres, followed by manipulations meant to capture porosity changes caused by densification or coarsening. Fig. 3 shows regions of typical packings. Monte-Carlo methods are used to form random-loose packings using spheres randomly chosen from a prescribed size distribution, such as monosize (Fig. 3a), Gaussian (Fig. 3b), or bimodal (Fig. 3c). These spheres are dropped into a large cylindrical "container" by releasing each sphere at a random position within the cylinder cross-section and allowing it to settle when it reaches a stable three-point contact. Spheres are not allowed to bounce or to move previously placed spheres. The resulting structures accurately capture the morphology of the void space formed during slow sedimentation or filtering of solids formed via condensation, precipitation, and combustion methods (cf. Figs. 2 and 3).

A quasi-spherical subset of this packing ($\sim 10^5$ spheres) is then extracted from this large cylindrical packing. For monosize spheres, the initial packing void fraction, ϕ, obtained by Monte-Carlo sampling of the void space is 0.42, consistent with values expected for random-loose structures (Haughey & Beveridge, 1969). Densification of agglomerates by compression or controlled sintering is achieved by randomly increasing the radii of the microspheres, using a uniform or Gaussian distribution, to achieve the desired void fraction. Examples of slightly densified ($\phi = 0.3$) and highly densified ($\phi = 0.05$) solids are shown in Figs. 3d and e,

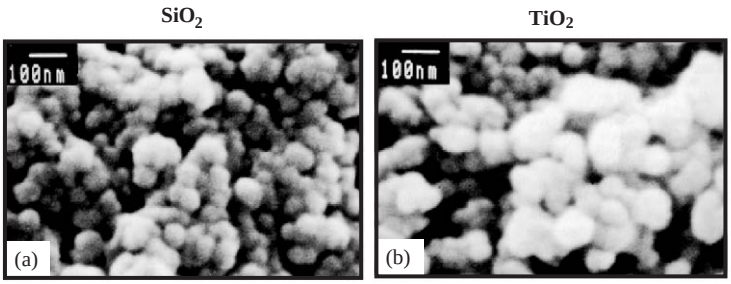

Fig. 2. Scanning electron micrographs of commonly used catalyst supports (a) SiO_2 and (b) TiO_2.

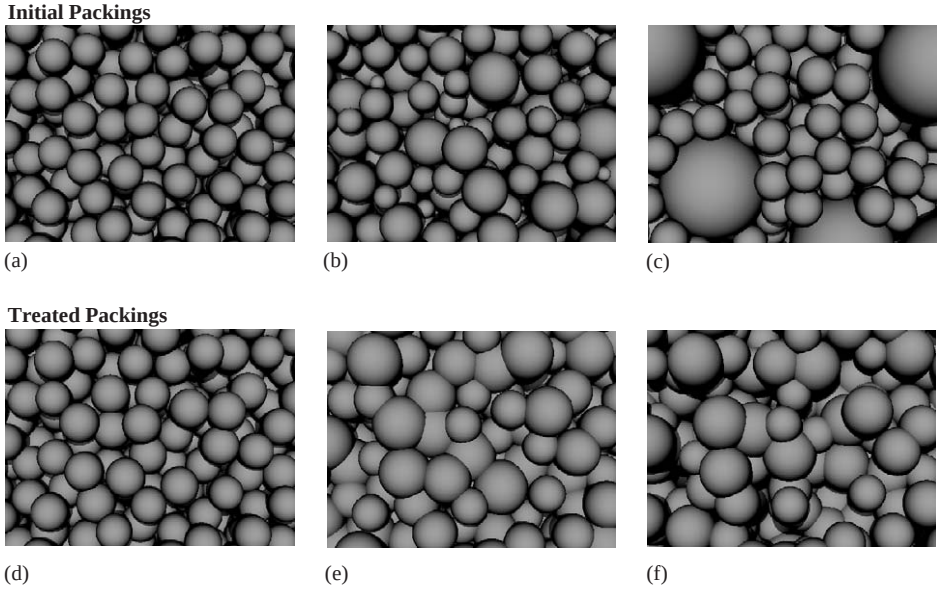

Fig. 3. Examples of model complex porous structures constructed with sphere packing and modification algorithms used in this study. Non-overlapped packings with unimodal (a), Gaussian (b), or bimodal (c) distributions of microsphere radii. Densified solids with void fractions of ϕ=0.3 (d) and ϕ=0.05 (e) and a coarsened solid with ϕ=0.3 (f).

respectively. Coarsening was simulated by randomly removing spheres from previously densified packings ($\phi = 0.05$) to reach the desired void fraction. Fig. 3f shows a sample of a coarsened solid with a void fraction of 0.3. This coarsening procedure leads to fewer and larger pores than in densified packings with similar void fractions (cf. Figs. 3d and f), as also detected by microscopy and porosimetry in coarsened and densified porous structures. The differences between densified and coarsened solids are apparent from volume-averaged pore size (radii) distributions determined from distances between collisions in Knudsen diffusion simulations (Fig. 4). For densified solids (Fig. 4a), normalized pore size distributions become narrower and shift toward smaller pores as densification occurs. Similar trends are apparent for coarsened solids (Fig. 4b), except that such solids exhibit broader pore size distributions, which shift toward larger pores than in densified solids with similar void fractions.

2.2. Transport simulation methods

2.2.1. Diffusion within voids

Tracers are initially placed at random positions within ~ 5 microsphere diameters of the packing center. Any molecule placed within a solid microsphere is assigned a zero displacement, while those started in void space are allowed to move as described below. Each simulation monitors the cumulative displacement of several thousand tracers, with a mean displacement, $\langle R \rangle$, of $\sim$ 10 microsphere diameters, while ensuring that the sample volume is large enough that fewer than 1% of the tracers reach the edge of the packing volume. These criteria enable sampling of representative void regions, while avoiding trajectories biased by the selective escape of those tracers that sample the structure most efficiently. In each simulation, we use an exponential distribution of free paths for gas phase redirecting collisions (Hildebrand, 1963), with a mean free path, λ, 100

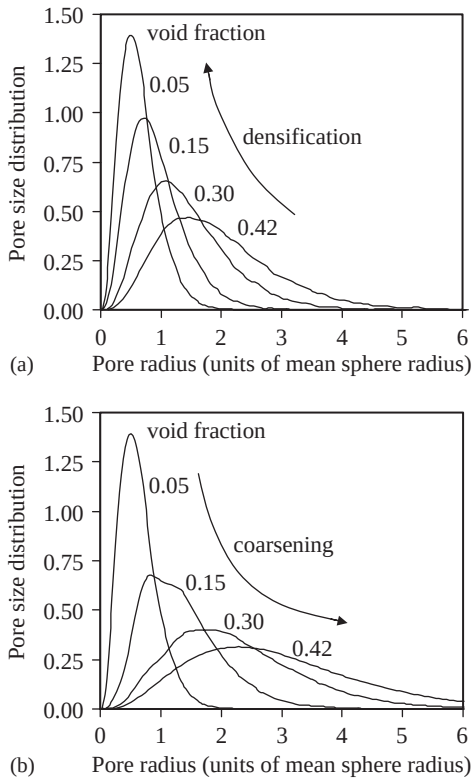

Fig. 4. Volume-based pore size (radii) distributions for densified (a) and coarsened (b) model porous structures. For each solid, the half-distances between successive wall collisions recorded during a Knudsen diffusion simulation were normalized by the mean sphere radius for that packing. The resulting values of normalized pore radii were binned and each bin count was weighted by the cube of the associated pore size.

times smaller than the mean pore radius, $\bar{r}_p$ (determined from the number-averaged distance between successive collisions in Knudsen diffusion simulations, $\lambda/\bar{r}_p > 10^2$). The small value of $\lambda/\bar{r}_p$ (0.01) ensures that diffusion occurs in the bulk regime. Tracers undergo random redirections after molecule–molecule collisions; the desorption direction after a molecule–wall collision is prescribed by the Knudsen cosine law (Greenwood, 2002; Knudsen, 1950). In our previous studies, (see Reyes & Iglesia, 1991a), desorption from a solid surface was assumed to occur in a purely random direction. As in our previous study, we use a hybrid continuum-discrete algorithm to increase computational efficiency. When a tracer is farther than $5 * \lambda$ from the nearest surface, it moves in one step to a random point on the surface of an imaginary sphere centered at the tracer position and tangent to that surface, and the simulation time is updated appropriately.

The effective diffusivity within the packing, $D_{e,g}$, is given by the Einstein equation in three dimensions:

$$D_{e,g} = \frac{\langle R^2 \rangle}{6t} \tag{4}$$

in which $\langle R^2 \rangle$ is the mean-square tracer displacement and t is the time elapsed; the latter is proportional to the total distance traveled by individual tracer steps. The geometric tortuosity factor, τ_g, for the void space is then given by

$$\tau_g = \frac{\phi \bar{D}}{D_{e,g}}. \tag{5}$$

Here, $\bar{D}$ is the diffusion coefficient in an equivalent capillary of radius $\bar{r}_p$. Because simulations are in the bulk regime, $\bar{D}$ equals $\lambda * v/3$, where v is the molecular velocity, taken to be unity here without loss of generality, but given rigorously for a given molecule by kinetic theory. The resulting tortuosity factor rigorously reflects the presence of redirecting obstacles, which lengthen the path between macroscopic points within complex porous structures.

2.2.2. Diffusion on the surface of packing spheres

Surface diffusion is simulated by monitoring the distance traveled by a few thousand tracers, constrained to move on exposed packing surfaces. Tracers are initially placed randomly on surfaces within the same central regions used in void space simulations. Each tracer is moved a fixed distance, λ_s, in a random direction during each Monte-Carlo step. The value of λ_s chosen is $0.01 * \bar{r}$, where $\bar{r}$ is the number-averaged microsphere radius. As discussed later, this value leads to normalized effective surface diffusivities and surface tortuosity estimates that do not depend on the value of λ_s.

Tracer motion on packing surfaces involves placing a tracer at a position (x_0, y_0, z_0) on the surface of sphere S_i, with radius R_i. The tracer is then moved a distance λ_s by choosing a random point on the circumference of the circle defined by the intersection of sphere S_i with an imaginary sphere of radius

$$\left(2R_i \sin\left(\frac{1}{2}\frac{\lambda_s}{R_i}\right)\right)$$

centered at the initial tracer location. This approach is valid for tracers located farther than a distance λ_s from the intersection of sphere S_i with its neighbors. Our choice of $\lambda_s = 0.01 * \bar{r}$ ensures that most steps can be described by this algorithm. At the new position (x_1, y_1, z_1) on sphere S_i, we use neighbor lists in order to determine whether the tracer resides within any of the spheres neighboring S_i. If point (x_1, y_1, z_1) does not fall within any of the neighbor spheres, a Monte-Carlo step is taken on sphere i. If point (x_1, y_1, z_1) is contained within a neighboring sphere, then that sphere (S_j) is chosen as the destination sphere. Rarely, a new point resides within two or more neighboring spheres, a situation that arises most frequently as void fractions approach the void percolation threshold ($\sim$0.04–0.05); in such cases, the closest sphere is arbitrarily chosen as the destination. Then, the tracer is returned to (x_0, y_0, z_0) and an acceptable destination is randomly chosen from the set of all exposed locations on S_j a distance of λ_s from (x_0, y_0, z_0). Surface diffusivities are estimated form the resulting mean square displacements $\langle R^2 \rangle$ of several thousand tracers covering representative

regions of the exposed surfaces of the packing ($\sim 10^7$ steps per tracer) using

$$D_{e,s} = \frac{\langle R^2 \rangle}{6t}. \quad (6)$$

The Einstein equation in three dimensions is used even though motion is restricted to exposed surfaces, because tracers sample the packing structure along all three coordinate axes, just as in diffusion within the void space.

An equivalent capillary is used to determine geometric tortuosities for the surface phase. Here, tracers are allowed to move on the surface of an infinitely long cylinder of radius $\bar{r}_p$ with the same step size λ_s as in the packing simulation. After sufficiently long times, surface diffusion on long capillaries becomes one dimensional, because only the axial dimension contributes to net displacements. Therefore, diffusivities are given by the one-dimensional Einstein equation ($D_{e,s} = \langle R^2 \rangle / 2t$). This capillary surface diffusivity is identical to that obtained for two-dimensional random walks on flat infinite planes and it is given by $\lambda_s * \nu/4$. Note that this diffusion coefficient would be a factor of two greater if exponentially distributed paths were used (Kennard, 1938); regardless of whether fixed or distributed jump distances are implemented, the same procedure must be used for the reference system as in the packing simulation. The equivalent capillary and an infinite plane provide identical references for determining surface tortuosities because

$$\tau_s = \frac{(\langle R^2 \rangle / 4t)_{\text{plane}}}{D_{e,s}} = \frac{(\langle R^2 \rangle / 2t)_{\text{capillary}}}{D_{e,s}}. \quad (7)$$

3. Results and discussion

3.1. Unbiased random walks on packing surfaces

The unbiased nature of the surface motion algorithm was confirmed by measuring the frequency with which tracers visit various surface regions in a subset of densified packings containing 20 microspheres. The surface of each sphere was described as a regular 50×50 grid spanning the θ and ϕ directions. Each of the 2500 patches on each sphere was described by its fractional exposure, estimated based on $\sim 10^8$ points randomly placed on each sphere. Patches partially exposed lie near intersections among spheres. A single tracer was allowed to move on the surface of the 20-sphere packing, taking 10^{10} steps of a size defined as a fraction of the average sphere radius $\bar{r}$. The number of visits (normalized by exposed patch area) was monitored for each patch. The resulting areal visitation frequencies are shown in Fig. 5 as a function of fractional exposure for a densified solid with void fractions of 0.3 (a) and 0.1 (b) and a $\lambda_s/\bar{r}$ of 0.01. For a void fraction of 0.3, the areal frequency was essentially constant for fractional exposures larger than ~ 0.25, but slightly smaller for patches at interfaces, which account for a very small fraction of exposed surfaces. This slight bias reflects the finite mean free path and the resulting non-statistical sampling of small patches by tracers. Visitation frequencies are less affected by fractional exposure for void fractions of 0.1 (Fig. 5b), because the fraction of the total exposed surface residing near intersections is much larger than for void fractions of 0.3; this leads to more representative sampling of partially exposed patches. For both void fractions, however, the use of a smaller jump distance (e.g. $\lambda_s = 0.002 * \bar{r}$) did not influence results. These data suggest that the algorithms used to describe motion on a sphere surface and crossing among spheres are unbiased.

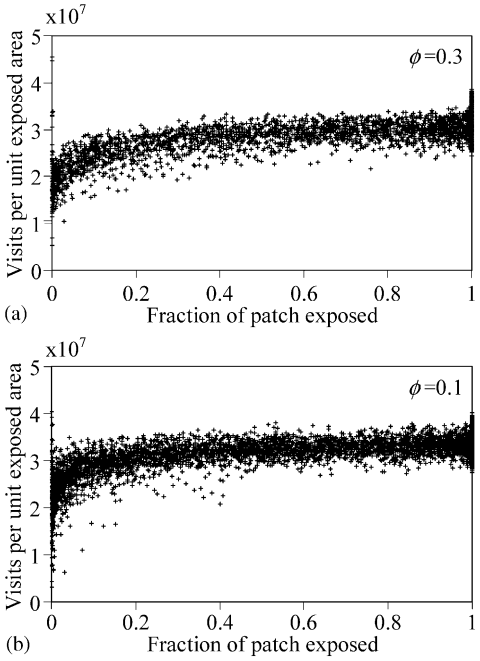

Fig. 5. Number of tracer visits per unit exposed surface area as a function of the fraction of patch area exposed for a single tracer moving on the surface of a 20-microsphere packing. Results are shown for packings densified to ϕ=0.3 (a) and ϕ=0.1 (b) and a fixed jump distance equal to 0.01 times the number-averaged sphere radius.

These conclusions were confirmed by the effective surface diffusivities determined for various step sizes ($\lambda_s/\bar{r}$). Fig. 6 shows normalized effective surface diffusivities, $D_{e,s}/(\lambda_s * \nu)$, as a function of $\lambda_s/\bar{r}$ for densified solids with void fractions of 0.1 and 0.3. Normalized diffusivities remained constant for step sizes up to $\lambda_s/\bar{r}$ of 0.40 and 0.20 for 0.3 and 0.1 void fractions, respectively. At even lower void fractions, the use of relatively large steps introduces difficulty in sphere crossing events, especially as typical pore dimensions become smaller with decreasing void fraction. Small steps, however, increase computational times required to cover representative packing regions. In view of this, we chose a $\lambda_s/\bar{r}$ value of 0.01 for surface diffusion simulations as a compromise between accuracy and computational efficiency.

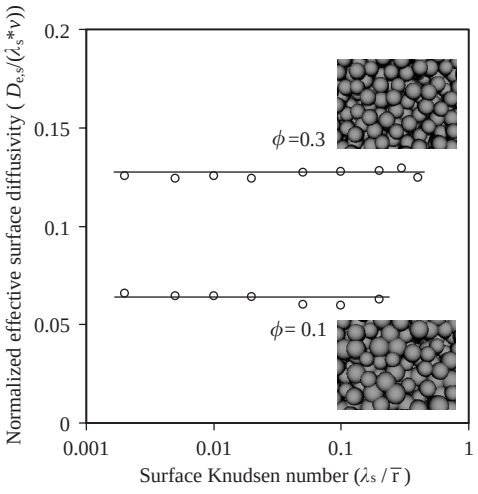

Fig. 6. Normalized effective surface diffusivities, $D_{e,s}/(\lambda_s * v)$, as a function of surface Knudsen number, defined as the ratio of the step size to the number-average sphere radius $\lambda_s/\bar{r}$, for densified packings with $\phi = 0.3$ and 0.1. Inset graphics show sample packing images for the corresponding model porous structures.

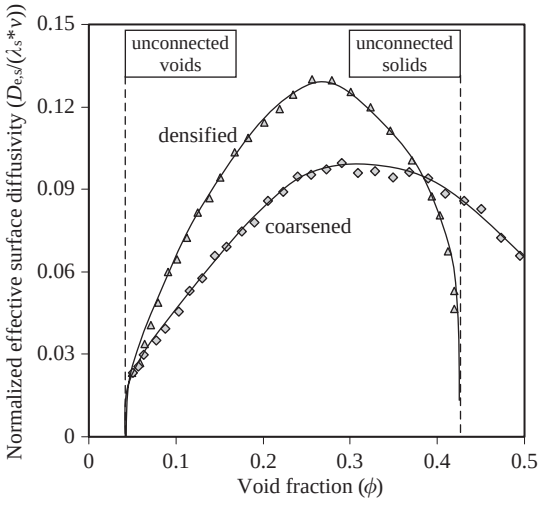

Fig. 7. Normalized surface diffusivities, $D_{e,s}/(\lambda_s * v)$, for densified and for coarsened solids as a function of void fraction. Vertical dashed lines indicate the void percolation threshold (unconnected voids) at $\phi \sim 0.04$–0.05, and the solid percolation threshold (unconnected surfaces) at $\phi \sim 0.42$ for the densified solid.

3.2. Surface and void phase transport in sphere packings

Here, we present simulation results for porous solids formed from initial random-loose packings of monosize spheres, which were densified to a given void fraction by increasing the sphere radii according to a uniform distribution. The structure and transport properties of such densified packings are essentially unaffected by whether microsphere growth is prescribed by uniform or Gaussian distributions. Fig. 7 shows normalized surface diffusivities, $D_{e,s}/(\lambda_s * v)$, for a wide range of void fractions,

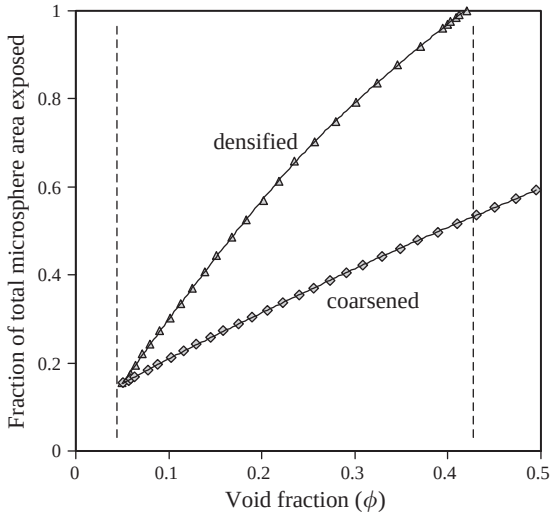

Fig. 8. The fraction of total microsphere surface area exposed for porous structures densified or coarsened to various void fractions.

achieved by either densification or coarsening. Effective surface diffusivities are obtained by multiplying these normalized surface diffusivities by the characteristic distance between binding sites and the surface mobility for a given molecule-surface system. Molecular dynamics simulations have been used to understand and predict the mobility of various species on well-defined surfaces (Baletto, Mottet, & Ferrando, 2000; Huang, Balan, Chen, & Fichthorn, 1994) and even on realistic amorphous solids (Stallons & Iglesia, 2001).

As expected, effective surface diffusivities increased with increasing void fraction (up to ~ 0.28) in densified solids because connecting surface paths among macroscopic regions become less contorted as void fraction increases. Larger void fractions, however, ultimately lead to loss of connectivity among sphere surfaces and to a decrease in effective diffusivity for packings with void fractions above 0.28. As void fractions approach values typical of contacting spheres (~ 0.42), macroscopic connectivity through the surface phase is lost and effective diffusivities approach zero as materials approach this solid percolation threshold. Coarsened solids show similar trends, but effective diffusivities do not drop as sharply at void fractions of ~ 0.42. This reflects the nature of the coarsening process, in which spheres are removed from very highly densified and well-connected packings; therefore, surface connectivity is retained even as we approach the percolation threshold for solids in random-loose packings. Fig. 8 shows the fraction of the total microsphere area that remains exposed after densification or coarsening to a given void fraction. Densification decreases the exposed surface fraction to 0.155 for a void fraction of 0.05 from its value of unity in the starting random-loose packing. As spheres are then removed from this densified packing in coarsening simulations, the fraction exposed increases but reaches only 0.525 (instead of unity) as the void fraction reaches that of

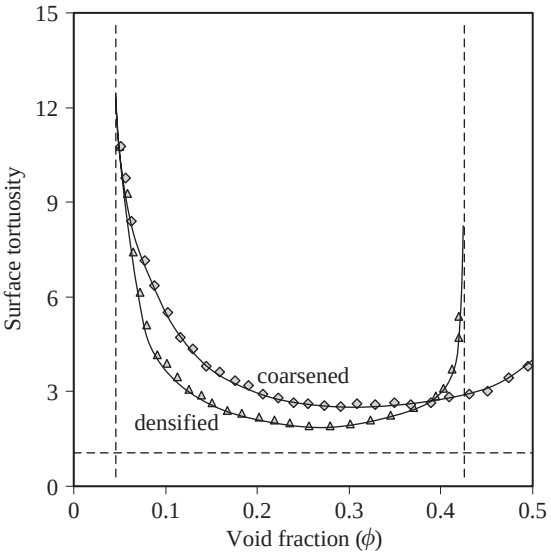

Fig. 9. Surface tortuosity factors for densified and coarsened porous structures as a function of void fraction.

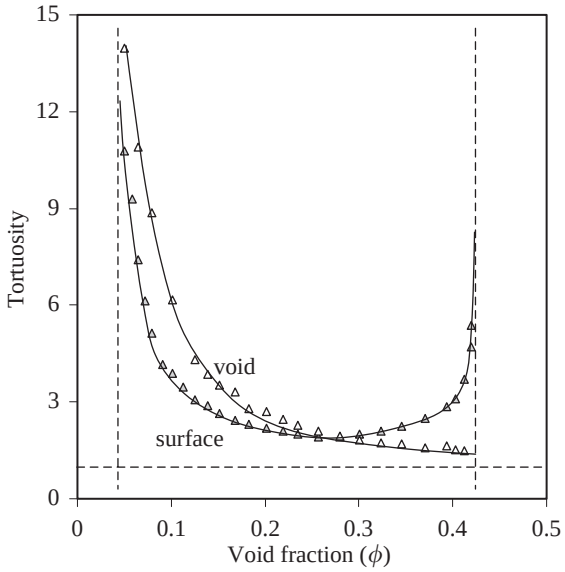

Fig. 10. Surface and void tortuosity factors for densified porous structures as a function of void fraction.

the initial random-loose packing (0.42). This illustrates the significant remaining connectivity of solids (and their surfaces) in coarsened porous structures even for large void fractions.

Tortuosity factors for the surface phase are shown in Fig. 9 for densified and coarsened solids as a function of void fraction. For densified solids, a minimum tortuosity factor of 1.9 is attained at a void fraction of ~ 0.26. Lower void fractions lead to larger surface tortuosities, which reach values of 7.4 at void fractions of 0.065 and continue to increase as the voids (and their defining surfaces) become disconnected for void fractions lower than 0.04–0.05. At such low void fractions, connected paths across macroscopic regions through the void space become unavailable and surface tortuosities concurrently approach infinite values. Thus, the sharp increase in surface tortuosity at low void fractions reflects the disappearance of a connected void phase and of its defining surface. Void fractions above ~ 0.26 lead also to high surface tortuosities, as the extent of overlap among neighboring spheres decreases, especially for densified solids. In fact, the surface phase becomes discontinuous with increasing void fraction; as a result, tracers are unable to cover macroscopic regions when constrained to move on surfaces. The surface phase becomes discontinuous at void fractions corresponding to the percolation threshold for the solid phase.

Coarsened solids exhibit similar trends for void fractions below 0.24, for which surface tortuosities increase as solids approach the void percolation threshold. Surface tortuosities, however, are higher than for densified solids with similar void fractions. This difference reflects the coarsening mechanism, in which removal of spheres from highly densified structures leads to more inaccessible regions than for similar void fractions achieved via densification processes, as discussed above. As in densified solids, surface tortuosities near the void percolation threshold in coarsened solids decrease with increasing void fraction and then increase as surface connectivity is lost at even higher void fractions. The relatively flat region of minimum tortuosity at intermediate void fractions is much broader for coarsened than for densified solids, because connectivity is retained at higher void fractions as a result of the highly densified solid from which coarsened solids are formed. Consequently, surface tortuosities in coarsened structures do not increase as sharply at void fractions above ~ 0.4 as in densified structures.

In an effort to relate surface and void space connectivities and transport properties, we compare next surface and void phase tortuosities for densified and coarsened model porous structures. The comparison is shown for densified solids in Fig. 10. Void tortuosity factors are higher than those for the surface phase for void fractions below ~ 0.25 (e.g., 4.28 vs. 2.65 at 0.15 void fraction; 12.25 vs. 5.12 at 0.08 void fraction). At void fractions higher than ~ 0.25, surface tortuosities become larger than for the void phase, as voids become increasingly connected at the expense of a decrease in the extent of sphere–sphere overlap. Fig. 11 shows similar comparisons for coarsened solids. Differences between surface and void phase tortuosities tend to be smaller for coarsened than for densified porous structures. At higher void fractions, surface tortuosities become again higher than for the void space. These similarities between void and surface phase tortuosities are reasonable when both phases are continuous, because the surface phase in effect defines every structural detail of the void space. To our knowledge, similar comparisons have not been previously reported for realistic complex porous structures.

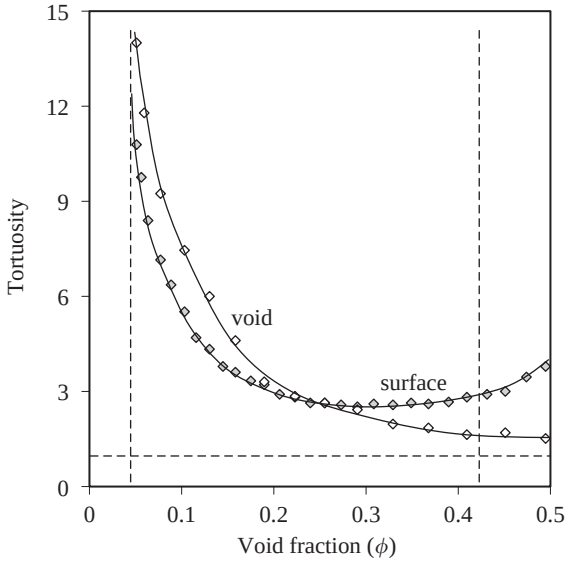

Fig. 11. Surface and void tortuosity factors for coarsened porous structures as a function of void fraction.

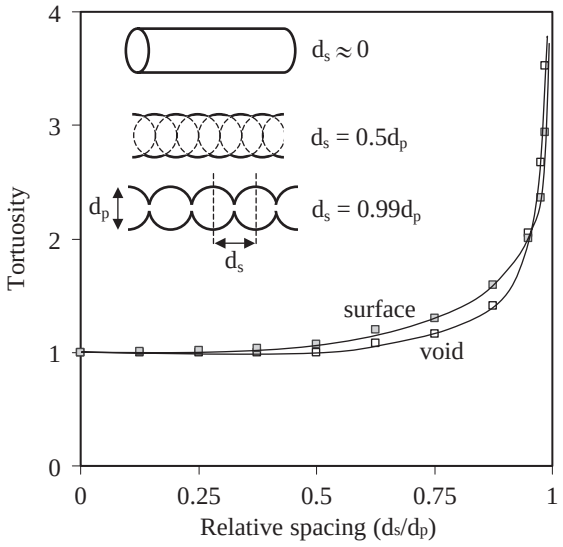

Fig. 12. Void and surface tortuosity factors as a function of relative spacing, d_s/d_p, for a periodically constricted pore system consisting of an infinite one-dimensional array of overlapping spheres.

The packings used in the previously discussed results were formed using initial packings of monosize spheres. Next, we explore the effects of the initial size distributions. Random-loose packings based on Gaussian size distributions with standard deviations of 0%, 5%, 10%, 15%, 20%, and 25% of the mean radius and truncated at three standard deviations were formed and densified to a void fraction of 0.3. Surface and void tortuosities were essentially independent of the breadth of the Gaussian distribution. For these cases, the void tortuosity factors vary by less than 2% from the value of 1.83 for monosize spheres; surface tortuosities for the Gaussian solids vary less than 3% from the value of 2.20 on initially monosize spheres. We also considered bimodal uniform solids containing equal volumes of spheres with radii r_1 and r_2. Size ratios of 1.0, 1.25, 1.57, 2.0, 2.5, 3.15, 3.97, and 5.0 were examined. For such bimodal solids, the void fraction of non-overlapping spheres decreased with increasing size ratio from a value of 0.42 for uniform spheres to 0.378 for $r_2/r_1 = 2.50$, and to 0.335 for $r_2/r_1 = 5.00$. After densification of each bimodal distribution to a void fraction of 0.3, void tortuosities differed by less than 5% from those for uniformly sized spheres ($r_2/r_1 = 1$), but surface tortuosities increased monotonically with increasing size ratio. For a void fraction of 0.3, surface tortuosities were 2.0 for uniformly sized spheres, 2.2 for $r_2/r_1 = 2.50$, and 2.37 for $r_2/r_1 = 5.00$. These small systematic differences between surface and void tortuosities reflect the lower extent of overlap required in order for a given packing to achieve a common void fraction of 0.3, in view of the lower initial void fraction achieved as the size ratio increased. In effect, densification to a given void fraction required less overlap as the size ratio increases, leading to larger values of surface tortuosities, which are very sensitive to the extent of sphere–sphere overlap.

3.3. Surface and void transport in an idealized pore system

Our algorithms for surface and void tracer diffusion were also used for model pore systems consisting of linear "necklaces" of partially overlapped spheres with diameter d_p with centers separated by a distance d_s (inset in Fig. 12). The voids are defined by the space contained within the spheres in the one-dimensional string. A given sequence of spheres is defined by its relative spacing, d_s/d_p. These void structures resemble a straight cylinder for d_s/d_p values near zero and a non-overlapping unconnected sequence of spheres for a values of unity. A similar construct was used previously (Kanellopoulos, Munday, & Nicholson, 1983; Nakano, Iwamoto, Yoshinaga, & Evans, 1987) in studies of Knudsen diffusion within periodically constricted pores.

Simulations of void space (in the bulk regime) and surface diffusion were carried out using the same algorithms described above for diffusion in the packings. Diffusivities were calculated from mean square displacements using the Einstein equation in one dimension, because net macroscopic displacements occur only along the axial direction. Fig. 12 shows void and surface tortuosities as a function of relative spacing, d_s/d_p, for this periodically constricted structure. As in the case of the packings, surface and void tortuosities are very similar and increase concurrently as the extent of overlap decrease and d_s/d_p values increase above 0.5. As the extent of overlap increases, the bicontinuous surface and void phases retain similar tortuosities, because the

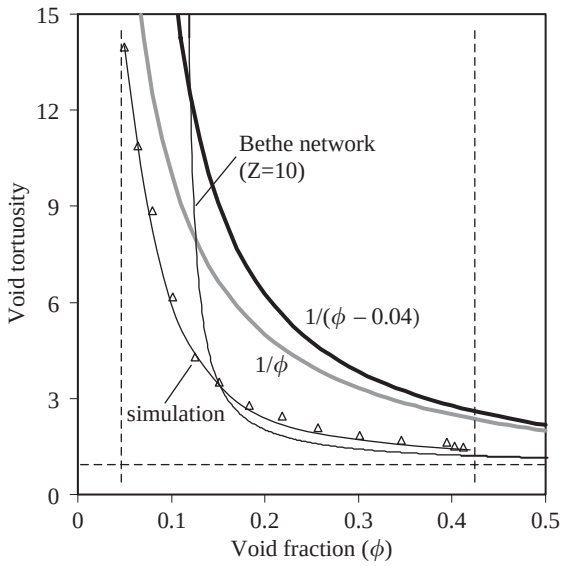

Fig. 13. Simulation results for void tortuosity based on bulk regime diffusion are compared with the $1/\phi$ form suggested by Wakao and Smith (1962), with $1/(\phi - 0.04)$, which is corrected for the void percolation threshold, and with results for a Bethe lattice with a coordination number of $Z = 10$.

structure of either phase exactly defines the other phase in a bicontinuous system.

3.4. Implications for description and understanding of pore structures

Tortuosity factors for void space are typically related to void fractions in porous structures using descriptions that neglect some essential structural features of the connecting paths (Mitani, 1984; Wakao & Smith, 1962). Theoretical analyses that lead to compact mathematical expressions for effective transport properties or void tortuosities often assume dilute or randomly placed spheres in a continuous second phase and assume that the void fraction captures all relevant geometrical features in a porous structure (Prager, 1963; Weissberg, 1963). Such approaches provide incomplete descriptions of complex porous solids typically used as adsorbents and catalysts. Fig. 13 shows again void tortuosities obtained from bulk diffusion simulations along with curves representing simple approximations of $\tau_g \sim 1/\phi$ and $\tau_g \sim 1/(\phi - 0.04)$; the latter form additionally captures that the tortuosity becomes infinite at the void percolation threshold, corresponding to a void fraction of ~ 0.04 for these solids. As seen in the graph, tortuosity values from these simple relations differ significantly from our estimates of void tortuosities, and would also fail to predict surface tortuosities in view of the topological correspondence between the surface and void space. As densification or coarsening occurs, pendant pores and isolated regions emerge as increasingly abundant components of the total void volume and contribute to effective diffusivities measured using tracer methods. Tracer methods, used here and in many experimental approaches, probe such pendant dead-end regions because tracers are "delayed" during the sampling of their volumes. Steady-state diffusivities, which are considerably more difficult to obtain experimentally and computationally, but which are relevant in many practical uses of these materials, are unaffected by such pendant voids because at steady-state net ingress into such regions does not occur. The differences between steady-state and tracer diffusion have been recognized (Bryntesson, 2002; Sotirchos, 1992). Steady-state diffusion simulations can be carried out using test-particle methods based on transmission probabilities (Abbasi, Evans, & Abramson, 1983; Burganos & Sotirchos, 1988) and we are currently implementing such simulations in our realistic packing structures.

The complexity of real and simulated porous structures and computational constraints hinder the measurement of the level of isolated or dead-end pore space in our model solids. Lattice-based structural models are amenable to analytical treatments of tortuosities, void isolation, and transport properties (Hollewand & Gladden, 1992; Reyes & Jensen, 1985; Sharratt & Mann, 1987; Vrettos, Imakoma, & Okazaki, 1989). One useful construct is a Bethe network consisting of a non-reconnecting infinite branching tree described fully by the number of branches emanating from each node (the coordination number Z). Porosity is introduced by removing a fraction of the branches and the effective diffusivities and various forms of porosity are obtained using analytical functions derived from percolation theory (see Reyes & Jensen, 1985). The non-reconnecting nature of the branches renders these models unphysical, but nonetheless useful in those cases where porous solids evolve as a result of chemical reactions. Fig. 13 shows the tortuosity-void fraction relation obtained for a connectivity value of 10, which provides the most reasonable agreement with tortuosity values obtained for our packings. Clearly, a lattice with fixed connectivity does not accurately represent void tortuosities throughout the entire range of void fractions, as expected from the much greater degree of isolation in non-reconnecting branches than in realistic void structures, especially as the void fraction approaches a percolation threshold. Even though Bethe lattices significantly overestimate the extent of porosity isolation, these lattice models predict that less than 30% of the total void fraction is isolated even for tortuosity factors of ~ 10. Therefore, our diffusion simulations in the much more extensively connected packing structures are unlikely to be affected by void isolation for the void fractions used throughout our simulations.

Next, we comment briefly about the void tortuosities in the bulk regime reported here and those obtained from Knudsen simulations using the number-averaged distance between collisions to estimate the equivalent capillary diffusivity. We find that void tortuosities are greater for Knudsen than for bulk diffusion, and their ratio increases as the void fraction decreases for both densified and coarsened solids. Even for

non-overlapping spheres, tortuosity factors are 2.09 and 1.48 in the Knudsen and bulk regimes, respectively, a finding that seems to indicate that a tortuosity factor as defined is not a true geometric property of the void (or surface) space. These differences become larger as the void fraction decreases; for example, the respective Knudsen and bulk tortuosity factors are 19.7 and 8.9 for a void fraction of 0.1. Similar discrepancies have been detected without clear resolution in transport simulations of random binary media (Burganos, 1998) and assemblies of capillaries (Burganos & Sotirchos, 1989) and for nuclear magnetic resonance experiments of diffusion in porous solids (Geier, Vasenkov, & Karger, 2002). We have concluded that such differences reflect the inappropriate use of an equivalent capillary Knudsen diffusivity evaluated as the number-averaged distance between collisions and not the geometric irrelevance of tortuosity factors. We are currently exploring rigorous averaging methods to describe the equivalent diffusivity. In view of this, we have focused the contents of this manuscript on effective diffusivities and tortuosities in the bulk diffusion regime, in which the distribution of distances between wall collisions is inconsequential to the mechanism and rate of transport in the void space, and for which the geometric relevance of tortuosity factors is unequivocal.

We conclude with some comments about the implications of the surface tortuosities reported here for our understanding of concurrent surface and void diffusion in porous structures. In contrast with processes involving exclusively diffusion in the fluid phase, for which kinetic theory or free-space diffusivities provide independent measures of mobility, diffusion on surfaces contains inseparable contributions from the mobility and the nature of the connecting paths. Mobility cannot be rigorously described with existing knowledge about surface chemistry and migration mechanisms, and cannot be independently measured on equivalent flat surfaces without significant concerns about fidelity. The length of the surface connecting path is not measurable without an independent assessment of surface mobility; the consequent absence of surface tortuosity measurements impedes our progress in understanding and predicting contributions from surface diffusion to overall transport within complex porous structures (Tsotsis, Sane, Webster, & Goddard, 1986). In this study, we have developed relations between void and surface tortuosities for solids with a given void fraction achieved via well-defined mechanisms for void formation and destruction (densification or coarsening). In practice, void tortuosities are experimentally accessible or can be estimated from void fractions using the simulations described here. Using additional data for surface tortuosities estimated from our simulation results, it is possible to extract surface mobilities for various molecules and a given porous structure using Eq. (3) and experimental effective surface diffusivities obtained from total transport rates properly corrected for the known contribution of diffusion processes in the voids. Together with independent measures of the surface-to-volume ratio (a_v), this provides a complete interpretation and a useful predictive framework for parallel diffusion in voids and surfaces within complex porous structures.

4. Conclusions

In the present work, we describe a new method for simulating surface diffusion and tortuosities in realistic complex porous structures. Simulations involve tracking mean-square displacements for many tracer molecules moving via random walks on exposed surfaces of packed and overlapped spheres. The unbiased nature of surface motion and sphere crossings was confirmed by rigorous statistics of areal visitation frequencies and by the irrelevance of jump distances on normalized diffusivities. Surface tortuosities in densified porous structures reached very large values at void fractions of 0.04 and 0.42, and a minimum value (1.9) at intermediate void fractions (~ 0.26). The large tortuosities at low and high void fractions correspond to the loss of continuity in the void and solid phases, respectively, both of which must be continuous in order to maintain a surface percolation path. Similar trends were obtained for porous solids made via coarsening algorithms, except that the solid phase becomes disconnected only at much higher void fractions, because coarsening procedures involve the random removal of spheres from a highly densified packing with significant solid connectivity. Simulations of bulk diffusion in the void space showed that tortuosity factors for the surface and the void phases are similar, except near the percolation threshold for the solid phase, for which higher void fractions allow motion through the voids but not through disconnected surfaces. A similar resemblance between the tortuosity of the voids and of their defining surfaces was found from simulations of transport in one-dimensional arrays of overlapped hollow spheres for all extents of sphere–sphere overlap. Comparisons with simple capillary and lattice models of porous structures reveal significant differences between the simulated tortuosities of complex porous structures and those estimated from these simple models. Our simulation results provide rigorous guidance for estimating effective diffusivities and tortuosities in both surface and void phases and for deconvoluting the dynamics of surface motion from the connectivity of the surface phase in experimental measurements of effective diffusivities in porous solids within which transport invariably occurs via parallel motion on the surface and in the intraparticle fluid phase.

Notation

a_v	surface-to-volume ratio
f_g	fugacity of the diffusing species in the gas phase
f_s	fugacity of the diffusing species in the surface phase

C_g	gas phase concentration, moles per unit void volume
C_s	surface concentration, moles per unit surface area
$\bar{D}$	equivalent diffusivity for calculation of void tortuosity
D_e	overall effective diffusivity
$D_{e,g}$	effective gas phase diffusivity
$D_{e,s}$	effective surface diffusivity
N	total flux
N_g	gas phase contribution to total flux
N_s	surface contribution to total flux
$\bar{r}$	number-averaged microsphere radius
$\bar{r}_p$	mean pore radius
$\langle R \rangle$	mean tracer displacement
$\langle R^2 \rangle$	mean-square tracer displacement
S_i	microsphere i
t	elapsed time
x	primary direction of species gradient
Z	coordination number for Bethe lattice

Greek letters

λ	mean free path for gas phase
λ_s	jump distance in surface simulations
v	gas molecular velocity or surface mobility
τ_g	gas (void) tortuosity
τ_s	surface tortuosity
ϕ	void fraction

Acknowledgements

The authors acknowledge the input of Jeanette M. Stallous and Chandrashekhar Sonwane in the development of draft versions of the surface diffusion algorithm.

References

Abbasi, M. H., Evans, J. W., & Abramson, I. S. (1983). Diffusion of gases in porous solids: Monte Carlo simulations in the Knudsen and ordinary diffusion regimes. *A.I.Ch.E. Journal*, *29*(4), 617–624.

Akanni, K. A., Evans, J. W., & Abramson, I. S. (1987). Effective transport coefficients in heterogeneous media. *Chemical Engineering Science*, *42*(8), 1945–1954.

Aris, R. (1975). *The mathematical theory of diffusion and reaction in permeable catalysts — Vol. 1: The theory of the steady state*. Oxford: Clarendon Press.

Ash, R., Barrer, R. M., & Pope, C. G. (1963). Flow of adsorbable gases and vapours in a microporous medium. I. Single sorbates. *Proceedings of the Royal Society of London Series A*, *271*(134), 1–18.

Baker, R. W. (2002). Future directions of membrane gas separation technology. *Industrial and Engineering Chemistry Research*, *41*(6), 1393–1411.

Baletto, F., Mottet, C., & Ferrando, R. (2000). Molecular dynamics simulations of surface diffusion and growth on silver and gold clusters. *Surface Science*, *446*(1–2), 31–45.

Barrer, R. M., & Grove, D. M. (1951a). Flow of gases and vapours in a porous medium and its bearing on adsorption problems. I. The steady state of flow. *Transactions of the Faraday Society*, *47*(8), 826–837.

Barrer, R. M., & Grove, D. M. (1951b). Flow of gases and vapours in a porous medium and its bearing on adsorption problems. II. Transient flow. *Transactions of the Faraday Society*, *47*(8), 837–844.

Bartholomew, C. H. (2001). Mechanisms of catalyst deactivation. *Applied Catalysis A: General*, *212*(1–2), 17–60.

Bhatia, S. K. (1988). Combined surface and pore volume diffusion in porous media. *A.I.Ch.E. Journal*, *34*(7), 1094–1105.

Bryntesson, L. M. (2002). Pore network modelling of the behaviour of a solute in chromatography media: Transient and steady-state diffusion properties. *Journal of Chromatography A*, *945*(1–2), 103–115.

Burganos, V. N. (1998). Gas diffusion in random binary media. *Journal of Chemical Physics*, *109*(16), 6772–6779.

Burganos, V. N., & Sotirchos, S. V. (1988). Simulation of Knudsen diffusion in random networks of parallel pores. *Chemical Engineering Science*, *43*(7), 1685–1694.

Burganos, V. N., & Sotirchos, S. V. (1989). Knudsen diffusion in parallel, multi-dimensional or randomly oriented capillary structures. *Chemical Engineering Science*, *44*(11), 2451–2462.

Carman, P. C., & Malherbe, P. L. (1950). Diffusion and flow of gases and vapours through micropores. II. Surface flow. *Proceedings of the Royal Society of London Series A*, *203*(1073), 165–178.

Choi, J.-G., Do, D. D., & Do, H. D. (2001). Surface diffusion of adsorbed molecules in porous media: Monolayer, multilayer, and capillary condensation regimes. *Industrial and Engineering Chemistry Research*, *40*(19), 4005–4031.

Dogu, T. (1981). The importance of pore structure and diffusion in the kinetics of gas-solid non-catalytic reactions: Reaction of calcined limestone with SO_2. *Chemical Engineering Journal and the Biochemical Engineering Journal*, *21*(3), 213–222.

Eberly Jr., P. E., & Vohsberg, D. B. (1965). Diffusion of benzene and inert gases through porous media at elevated temperatures and pressures. *Transactions of the Faraday Society*, *61*(516P), 2724–2735.

Froment, G. F., & Bischoff, K. B. (1990). *Chemical reactor analysis and design* (2nd ed.). New York: Wiley.

Geier, O., Vasenkov, S., & Karger, J. (2002). Pulsed field gradient nuclear magnetic resonance study of long-range diffusion in beds of NaX zeolite: Evidence for different apparent tortuosity factors in the Knudsen and bulk regimes. *Journal of Chemical Physics*, *117*(5), 1935–1938.

Gilliland, E. R., Baddour, R. F., Perkinson, G. P., & Sladek, K. J. (1974). Diffusion on surfaces. I. Effect of concentration on diffusivity of physically adsorbed gases. *Industrial and Engineering Chemistry Fundamentals*, *13*(2), 95–100.

Greenwood, J. (2002). The correct and incorrect generation of a cosine distribution of scattered particles for Monte-Carlo modelling of vacuum systems. *Vacuum*, *67*(2), 217–222.

Haughey, D. P., & Beveridge, G. S. (1969). Structural properties of packed beds—a review. *Canadian Journal of Chemical Engineering*, *47*(2), 130–140.

Hildebrand, J. H. (1963). *An introduction to kinetic theory*. New York: Reinhold.

Ho, F.-G., & Strieder, W. (1981). A variational calculation of the effective surface diffusion coefficient and tortuosity. *Chemical Engineering Science*, *36*(2), 253–258.

Hollewand, M. P., & Gladden, L. F. (1992). Representation of porous catalysts using random pore networks. *Chemical Engineering Science*, *47*(9–11), 2757–2762.

Holyst, R., Plewczynski, D., Aksimentiev, A., & Burdzy, K. (1999). Diffusion on curved, periodic surfaces. *Physical Review E*, *60*(1), 302–307.

Huang, D., Balan, P. G., Chen, Y., & Fichthorn, K. A. (1994). Molecular-dynamics simulation of the surface-diffusion of *n*-alkanes on Pt(111). *Molecular Simulation*, *13*(4–5), 285–298.

Jaguste, D. N., & Bhatia, S. K. (1995). Combined surface and viscous-flow of condensable vapor in porous-media. *Chemical Engineering Science*, *50*(2), 167–182.

Kanellopoulos, N., Munday, K. A., & Nicholson, D. (1983). The flow of a non-adsorbed, collisionless gas through linked spheres—a model for zeolite diffusion. *Journal of Membrane Science*, *13*(2), 247–258.

Kennard, E. H. (1938). *Kinetic theory of gases*. New York: McGraw-Hill.

Knudsen, M. (1950). *The kinetic theory of gases: Some modern aspects* (3rd ed.). New York: Wiley.

Kong, C. S., Kim, D. Y., Lee, H. K., Shul, Y. G., & Lee, T. H. (2002). Influence of pore-size distribution of diffusion layer on mass-transport problems of proton exchange membrane fuel cells. *Journal of Power Sources*, *108*(1–2), 185–191.

Lee, H. H. (1985). *Heterogeneous reactor design*. Boston: Butterworth.

Mitani, M. (1984). Geometric factor for diffusion in porous media. *Journal of Chemical Engineering of Japan*, *17*(4), 441–443.

Nakano, Y., Iwamoto, S., Yoshinaga, I., & Evans, J. W. (1987). The effect of pore necking on Knudsen diffusivity and collision frequency of gas molecules with pore walls. *Chemical Engineering Science*, *42*(7), 1577–1583.

Pekalski, A., & Ausloos, M. (1995). Surface tracer diffusion in the presence of a solid barrier: A Monte Carlo study. *Surface Science*, *344*(3), L1271–L1274.

Prager, S. (1963). Diffusion and viscous flow in concentrated suspensions. *Physica*, *29*(2), 129–139.

Prasetyo, I., Do, H. D., & Do, D. D. (2002). Surface diffusion of strong adsorbing vapours on porous carbon. *Chemical Engineering Science*, *57*(1), 133–141.

Raimondeau, S., & Vlachos, D. G. (2002). Recent developments on multiscale, hierarchical modeling of chemical reactors. *Chemical Engineering Journal*, *90*(1–2), 3–23.

Reed Jr., E. M., & Butt, J. B. (1971). Surface diffusion of single sorbates at low and intermediate surface coverage. *Journal of Physical Chemistry*, *75*(1), 133–141.

Reyes, S. C., & Iglesia, E. (1991a). Effective diffusivities in catalyst pellets—new model porous structures and transport simulation techniques. *Journal of Catalysis*, *129*(2), 457–472.

Reyes, S. C., & Iglesia, E. (1991b). Monte-Carlo simulations of structural properties of packed beds. *Chemical Engineering Science*, *46*(4), 1089–1099.

Reyes, S. C., & Iglesia, E. (1993). Simulation techniques for the design and characterization of catalyst pellets. In R. E. Becker, & C. J. Pereira (Eds.), *Computer aided design of catalysts* (p. 89). New York: Marcel Dekker.

Reyes, S. C., & Jensen, K. F. (1985). Estimation of effective transport coefficients in porous solids based on percolation concepts. *Chemical Engineering Science*, *40*(9), 1723–1734.

Reyes, S. C., Sinfelt, J. H., & DeMartin, G. J. (2000). Diffusion in porous solids: The parallel contribution of gas and surface diffusion in pores extending from the mesoporous region into the microporous region. *Journal of Physical Chemistry B*, *104*(24), 5750–5761.

Richard, V., Favre, E., Tondeur, D., & Nijmeijer, A. (2001). Experimental study of hydrogen, carbon dioxide and nitrogen permeation through a microporous silica membrane. *Chemical Engineering Journal*, *84*(3), 593–598.

Ruthven, D. M. (1984). *Principles of adsorption and adsorption processes*. New York: Wiley.

Satterfield, C. N. (1970). *Mass transfer in heterogeneous catalysis*. Cambridge, MA: MIT Press.

Schneider, P., & Smith, J. M. (1968). Chromatographic study of surface diffusion. *A.I.Ch.E. Journal*, *14*(6), 886–895.

Sharratt, P. N., & Mann, R. (1987). Some observations on the variation of tortuosity with Thiele modulus and pore size distribution. *Chemical Engineering Science*, *42*(7), 1565–1576.

Somorjai, G. A. (1972). *Principles of surface chemistry*. Englewood Cliffs, NJ: Prentice-Hall, Inc.

Sotirchos, S. V. (1992). Steady-state versus transient measurement of effective diffusivities in porous-media using the diffusion-cell method. *Chemical Engineering Science*, *47*(5), 1187–1198.

Stallons, J. M., & Iglesia, I. (2001). Simulations of the structure and properties of amorphous silica surfaces. *Chemical Engineering Science*, *56*(14), 4205–4216.

Tomadakis, M. M., & Sotirchos, S. V. (1993). Ordinary, transition, and Knudsen regime diffusion in random capillary structures. *Chemical Engineering Science*, *48*(19), 3323–3333.

Tsong, T. T. (2001). Mechanisms of surface diffusion. *Progress in Surface Science*, *67*(1–8), 235–248.

Tsotsis, T. T., Sane, R. C., Webster, I. A., & Goddard, J. D. (1986). Theoretical and experimental aspects of surface-diffusion in porous catalysts. I. Nonreactive conditions. *Journal of Catalysis*, *101*(2), 416–427.

Tuchlenski, A., Uchytil, P., & Seidel-Morgenstern, A. (1998). An experimental study of combined gas phase and surface-diffusion in porous glass. *Journal of Membrane Science*, *140*(2), 165–184.

Vrettos, N. A., Imakoma, H., & Okazaki, M. (1989). Transport-properties of porous-media from the microgeometry of a three-dimensional Voronoi network. *Chemical Engineering and Processing*, *26*(3), 237–246.

Wakao, N., & Smith, J. M. (1962). Diffusion in catalyst pellets. *Chemical Engineering Science*, *17*(11), 825–834.

Weissberg, H. L. (1963). Effective diffusion coefficient in porous media. *Journal of Applied Physics*, *34*(9), 2636–2639.

Weisz, P. B., & Hicks, J. S. (1962). The behaviour of porous catalyst particles in view of internal mass and heat diffusion effects. *Chemical Engineering Science*, *17*(4), 265–275.

Wen, C. Y. (1968). Noncatalytic heterogeneous solid fluid reaction models. *Industrial and Engineering Chemistry*, *60*(9), 34–54.